

The observed radio/gamma-ray emission correlation for blazars with the *Fermi*-LAT and the RATAN-600 data

T. Mufakharov,^{1*} M. Mingaliev,^{1,2} Yu. Sotnikova,¹ Ya. Naiden¹ and A. Erkenov¹

¹Special Astrophysical Observatory of RAS, Nizhnij Arkhyz, 369167 Russia

²Kazan Federal University, 18 Kremlyovskaya St., Kazan, 420008, Russia

Accepted 2015 April 6. Received 2015 March 18; in original form 2014 September 25

ABSTRACT

We study the correlation between gamma-ray and radio band radiation for 123 blazars, using the *Fermi*-LAT first source catalog (1FGL) and the RATAN-600 data obtained at the same period of time (within a few months). We found an apparent positive correlation for BL Lac and flat-spectrum radio quasar (FSRQ) sources from our sample through testing the value of the Pearson product-moment correlation coefficient. The BL Lac objects show higher values of the correlation coefficient than FSRQs at all frequencies, except 21.7 GHz, and at all bands, except 10 – 100 GeV, typically at high confidence level ($> 99\%$). At higher gamma-ray energies the correlation weakens and even becomes negative for BL Lacs and FSRQs. For BL Lac blazars, the correlation of the fluxes appeared to be more sensitive to the considered gamma-ray energy band, than to the frequency, while for FSRQ sources the correlation changed notably both with the considered radio frequency and gamma-ray energy band. We used a data randomization method to quantify the significance of the computed correlation coefficients. We find that the statistical significance of the correlations we obtained between the flux densities at all frequencies and the photon flux in all gamma-ray bands below 3 GeV is high for BL Lacs (chance probability $\sim 10^{-3} - 10^{-7}$). The correlation coefficient is high and significant for the 0.1 – 0.3 GeV band and low and insignificant for the 10 – 100 GeV band for both types of blazars for all considered frequencies.

Key words: galaxies: active – BL Lacertae objects: general – radiation mechanisms: non-thermal – gamma-rays: general – radio continuum: general

1 INTRODUCTION

Blazars are the most extreme class of active galactic nuclei (AGNs) characterized by a prominent jet pointing within a few degrees of our line of sight (Urry & Padovani 1995). They are known to be highly variable at gamma-ray wavelengths, as well as in the radio band, on time scales of days to months (von Montigny et al. 1995). Observationally they are divided into two main classes: the BL Lac objects (BL Lacs) with an almost featureless spectrum and the flat-spectrum radio quasars (FSRQs) with strong broad emission lines in their spectrum (Urry & Padovani 1995).

The spectral energy distribution (SED) of blazars is characterized by two broad features. The first one, peaking at lower energy, is generally explained in terms of synchrotron emission; the second feature, peaking at higher energies, is likely due to inverse Compton radiation (Sambruna, Maraschi & Urry 1996). Most of the observed radio to optical (and in some cases X-ray) emission from the blazars is due to synchrotron radiation in the jet (Bregman et al. 1981; Urry & Mushotzky 1982; Impey & Neugebauer 1988; Marscher 1998). Synchrotron emission is produced by relativistic

electrons, moving in a magnetic field (Rybicki & Lightman 1979). Inverse Compton photons originate from the interaction of the energetic electrons with seed photons. These seed photons could be produced by synchrotron emission, via synchrotron self-Compton (SSC) radiation (e.g., Konigl 1981; Marscher & Gear 1985), or they might originate from some external source - in this case it is external inverse Compton radiation (e.g., Sikora, Begelman & Rees 1994; Blandford & Levinson 1995). The gamma-ray photons could originate through the SSC mechanism, and then one might expect significant correlation between gamma-ray and radio emission because of the same origin for the radio and gamma-ray photons. On the other hand, if there is no reliable proof for such connection, that would support the theory of the independent origin of these emissions.

Since the majority of AGNs identified with gamma-ray sources are also bright radio sources - about half of the 1400 gamma-ray sources from the first *Fermi*-LAT catalogue (Abdo et al. 2010b) were identified with radio sources - this provides the motivation to search for a correlation between radiation in gamma-ray and radio bands. By investigating such correlation one can study time delays between the different events in the gamma-ray and radio band light curves, the physical processes and the characteristics

* E-mail: timur.mufakharov@gmail.com;

of the radiation in the AGN jets. The presence or absence of correlation also can help to more accurately determine the parameters of the models for the structure and processes in AGNs.

The first dedicated studies of the gamma-ray-radio emission correlation in blazars were based on EGRET data (e.g., [Stecker, Salamon & Malkan 1993](#); [Padovani et al. 1993](#)). However, these results remain uncertain due to the use of observational data obtained non-simultaneously, and also because samples were flux limited ([Muecke et al. 1997](#); [Taylor et al. 2007](#)).

The search for significant correlation between gamma-ray and radio emission continued, when *Fermi*-LAT telescope data became available. Using gamma-ray data from EGRET and *Fermi* surveys, [Ghirlanda et al. \(2010\)](#) noted that flux could change up to three times during the year. When average flux values are used for analysis, short-term variability (from one to several days or weeks) did not greatly affect the variability averaged over the year. The $F_\gamma - F_r$ correlation has been studied by [Ghirlanda et al. \(2010\)](#) between the gamma-ray flux above 100 MeV (using 1FGL catalogue; [Abdo et al. 2010c](#)) and the 20 GHz flux density (using ATCA survey; [Murphy et al. 2010](#)). A statistically significant (more than 3σ) correlation was found both for the population of BL Lac and FSRQ sources. Also they considered selection effects (sensitivity limits for radio and gamma-ray telescopes) and the likelihood that some radio sources were not detected due to their variability in the gamma-ray band.

[Kovalev et al. \(2009\)](#) also investigated the correlation between radio emission and gamma-ray flux (using *Fermi*-LAT data after the first three months of observations) for 135 AGNs. The non-parametric Kendall tau test confirmed a positive correlation at a confidence level greater than 99.9 % between the gamma-ray flux (for the 100 MeV-1 GeV energy band) and radio flux density (measured by the Very Long Baseline Array at 15 GHz within several months of the *Fermi*-LAT observations). The same analysis for the second *Fermi*-LAT energy band, 1 – 100 GeV, also showed a positive correlation, but at a lower confidence level - 86 %.

[Ackermann et al. \(2011\)](#) performed a detailed statistical analysis of the correlation between the radio and gamma-ray emission of the AGNs detected by *Fermi*-LAT in its first year of operation. For the radio band they used archival data at 8 GHz for 599 sources and concurrent measurements at 15 GHz for 199 sources, provided by the Owens Valley Radio Observatory monitoring programme ([Richards et al. 2011](#)). One distinctive feature of that work was the study of not only the *apparent*, but also the *intrinsic* strength of the correlation, exploiting a new statistical method by [Pavlidou et al. \(2012\)](#). They found that the statistical significance of a positive correlation between the centimetre radio and the broadband ($E > 100$ MeV) gamma-ray energy flux is very high for both flat spectrum radio quasars and BL Lac objects from their AGN sample.

Moreover, the correlation between high frequency radio emission (at 37 GHz) and gamma-ray emission (100 MeV-100 GeV *Fermi*-LAT data) for 249 northern AGNs was studied by [Niépola et al. \(2011\)](#). They also found a significant correlation between both the flux densities and luminosities in the gamma-ray and radio bands and suggested that the gamma radiation is produced co-spatially with the 37 GHz emission, i.e. in the jet.

On the basis of the work, considered above, it can be concluded that homogeneous (derived from one instrument) and simultaneous observational data in the radio and gamma-ray bands are essential for detection a possible correlation in radiation from blazars.

In this paper we present a statistical analysis of the correlation between radio and gamma-ray emission for a sample of 123 blazars

using quasi-simultaneous observational data from the *Fermi*-LAT and the RATAN-600 telescopes. The correlation analysis was performed using the flux densities from five radio bands, 21.7, 11.2, 7.7, 4.8 and 2.3 GHz, for the first time.

2 SAMPLE SOURCES AND OBSERVATION

For the correlation analysis we cross-match the first *Fermi*-LAT catalogue (1FGL) with the RATAN-600 observations. The 1FGL catalogue is available in the Vizier database¹ and its description is given in [Abdo et al. \(2010b\)](#). The catalogue includes observational data obtained during the period from 2008 August 4 to 2009 July 4 for 1451 AGNs and contains information for five gamma-ray bands: 0.1 – 0.3, 0.3 – 1, 1 – 3, 3 – 10 and 10 – 100 GeV. Gamma-ray flux units are photons per second per square centimetre ($\text{ph cm}^{-2} \text{s}^{-1}$). The counts in each band are averaged over 11 months.

About 300 AGNs were observed with the RATAN-600 radio telescope within a few months of the *Fermi*-LAT observations, as part of various programmes. For the analysis we used flux densities measured at five frequencies (2.3, 4.8, 7.7, 11.2 and 21.7 GHz) in 2008 November and 2009 April. Each source was observed 5 to 10 times during this period. The experimental data were processed with the modules of the FADPS (Flexible Astronomical Data Processing System) standard reduction package by [Verkhodanov \(1997\)](#). The processing methods are described in the paper by [Mingaliev et al. \(2012\)](#). The following 12 flux density calibrators (standard and RATAN's traditional ones) were used to get the coefficients of antenna elevation: 3C48, 3C138, 3C147, 3C161, 3C286, 3C295, 3C309.1, NGC7027, J0237–23, J1154–35, J1347+12 and J0410+76. Measurements of some calibrators were corrected for angular size and linear polarization, following the data summarized in [Ott et al. \(1994\)](#) and [Tabara & Inoue \(1980\)](#), respectively. The detection limit for the RATAN-600 single sector is approximately 8 mJy (integration time is about 3 s) under good weather conditions at the frequency of 4.8 GHz and at an average antenna elevation ($\delta \sim 42^\circ$). The detection limits at other frequencies are presented in Table 1 along with the other parameters of radiometers: f_0 – central frequency, Δf_0 – bandwidth, ΔF – flux density detection limit per beam, and BW – beam width [full width at half-maximum (FWHM) in right ascension (RA)] at average antenna elevation ($\delta \sim 42^\circ$). Beam width in declination is three to five times worse than in RA. These values depend on the atmospheric extinction instability and the effective area at the antenna elevation H (from 10° up to 90° above the horizon) at the corresponding frequencies. Radio data that are used in this paper are published in RATAN-600 BL Lacs database² ([Mingaliev et al. 2014](#)) and in [Mingaliev et al. \(2012\)](#). Standard errors in determining the flux density for these data are 7-8 % at 2.3 GHz and 4-5 % at other frequencies. Almost all of the sources had relatively strong flux levels at radio frequencies with a signal-to-noise ratio $S/N \geq 4$.

After cross-matching we had 123 AGNs for which quasi-simultaneous *Fermi*-LAT and RATAN-600 data were available. They make up the final list for the further analysis. In Table 2 we present: source name [from the NASA/IPAC (NED)³ or from

¹ <http://vizier.u-strasbg.fr/>

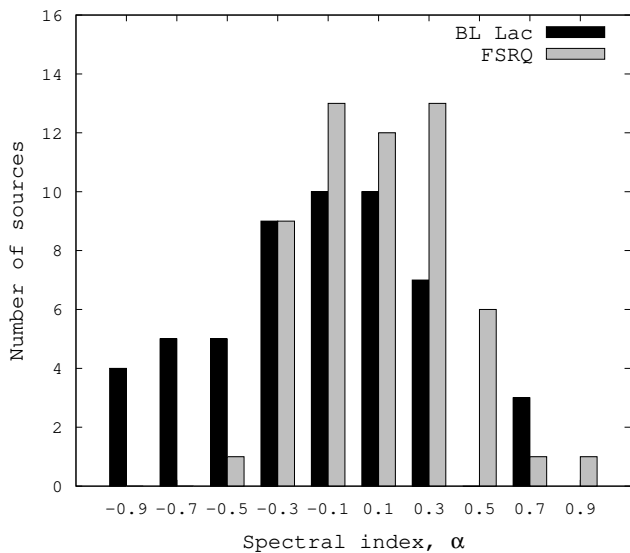
² <http://www.sao.ru/blcat/>

³ <http://ned.ipac.caltech.edu/>

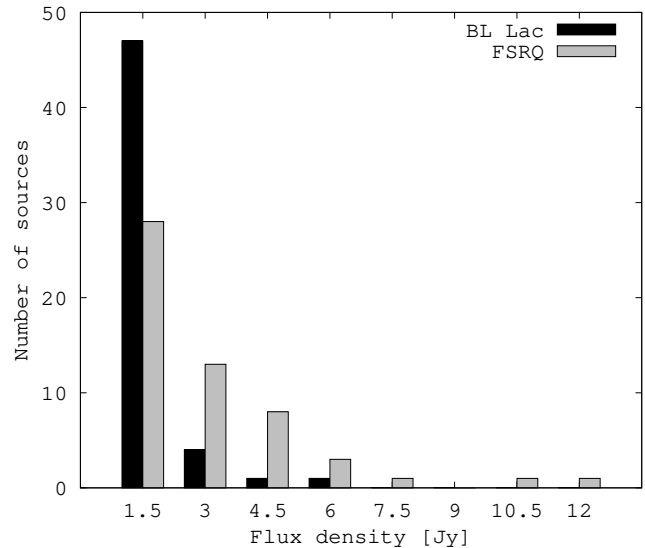
Table 1. RATAN-600 continuum radiometers.

f_0 (GHz)	Δf_0 (GHz)	ΔF (mJy beam ⁻¹)	BW (arcsec)
21.7	2.5	70	11
11.2	1.4	20	16
7.7	1.0	25	22
4.8	0.9	8	36
2.3	0.4	30	80

Column designation: Col. 1 – central frequency, Col. 2 – bandwidth, Col. 3 – flux density detection limit per beam, and Col. 4 – beam width (FWHM in RA).


Figure 1. Distribution of the spectral indices, measured between 2.3 and 7.7 GHz for BL Lacs (shown with black) and FSRQs (shown with grey)

the Roma-BZCAT catalogue⁴ (Massaro et al. 2009)] (column 1), blazar type (Roma-BZCAT) (column 2), and redshift value (NED) (column 3). There are different sub-classes of blazars presented in this sample: 53 – BL Lacs, 6 – BL Lac candidates, 8 – blazars of uncertain type, 56 – FSRQs. Almost all FSRQs and most of the BL Lacs have a flat radio spectrum ($|\alpha| \leq 0.5$), Figure 1 shows the spectral index distribution for FSRQs and BL Lacs from our sample. Figure 2 shows the distribution of flux densities, measured at 4.8 GHz, for BL Lacs and FSRQs (we exclude 3C 273 ($F > 39$ Jy) from this distribution for clarity of the display). The flux density does not reach 1 Jy for most of the BL Lacs at all frequencies. Note that FSRQs, observed with the RATAN-600, are limited by flux density (≥ 1 Jy). Moreover the representation of BL Lacs in our sample is incomplete, since they were observed partly in different programmes. In Table 3, we list the radio flux densities at different frequencies used in this work, along with the spectral index values (α), measured between 2.3 and 7.7 GHz, but for two sources measured between 4.8 and 7.7 GHz (due to the absence of observations at 2.3 GHz for them).


Figure 2. Distribution of the flux densities at 4.8 GHz, measured with the RATAN-600, for BL Lacs (shown with black) and FSRQs (shown with grey). We note that flux density does not reach 1 Jy for most of the BL Lacs

3 RESULTS

3.1 Flux density correlation

With the broadband observational data available for radio and gamma-ray bands, we compared correlation coefficients for a relatively large and approximately equal number of sources from two blazar sub-classes (BL Lacs and FSRQs). We checked the possibility of the existence of the flux density correlation measured at five radio bands with photon flux in five gamma-ray bands. We calculate the Pearson product-moment correlation coefficient r between radio and gamma-ray flux for the objects of our sample. In Table 4 we present correlation coefficients for five radio and five gamma-ray bands, along with the number of sources (N) with available radio data at each frequency (we have data for the full sample in gamma-rays) and typical confidence level values (CL) for calculated correlation coefficients for each considered band. Figures 4 - 8 are $F_\gamma - F_r$ plots. The sub-samples are plotted with different symbols: BL Lac - empty circles, FSRQ - filled triangles, BL Lac candidates - empty squares, blazar of uncertain type - filled squares.

In Figure 3 we visualize the correlation coefficients, reported in Table 4. In this figure, the correlation coefficients are shown across the five energy bands and for each of the five frequencies. The accuracy, to which the correlation coefficients are determined, is shown by the error bars, which correspond to the standard deviation defined as in Wall & Jenkins (2003): $\sigma_r = (1 - r^2) / (\sqrt{N} - 1)$ where N is the number of objects and r is the Pearson product-moment correlation coefficient.

The correlation coefficient is sensitive to both radio frequency and gamma-ray energy band. The correlation coefficient decreases with increasing energy band for both BL Lacs and FSRQs. Also it can be seen from Figure 3 that this fall is greater for BL Lacs. On average, correlation coefficients are higher for BL Lacs; and comparable values for BL Lacs and FSRQs are obtained only when the 21.7 GHz frequency band is considered.

For both types of sources we found a common trend: the highest correlation of the flux densities at all radio frequencies was detected with the 0.1 – 0.3 GeV gamma-ray band flux. Larger cor-

⁴ <http://www.asdc.asi.it/bzcat/>

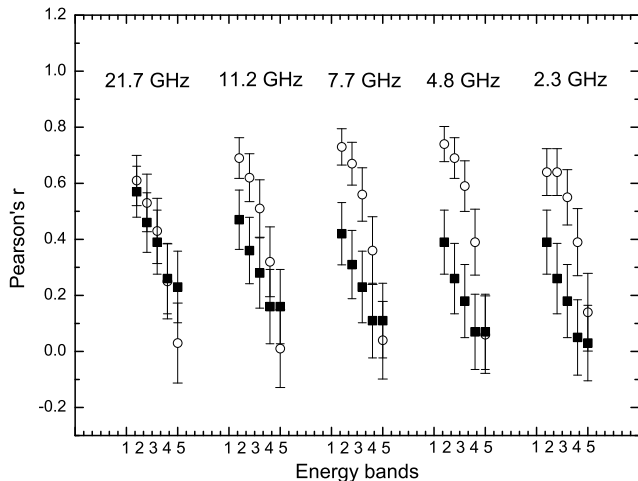


Figure 3. Pearson’s r distribution for the radio flux density and gamma-ray photon flux as a function of the energy bands shown for five frequencies. Correlation coefficients shown with empty circles for BL Lacs and with filled squares for FSRQs. Five energy bands are marked with numbers 1–5 (0.1–0.3, 0.3–1, 1–3, 3–10, and 10–100 GeV, respectively) in a horizontal axis for each frequency: 21.7, 11.2, 7.7, 4.8 and 2.3 GHz. Plotted values of the Pearson’s r are from Table 4

relation coefficients occur for BL Lacs than for FSRQs at all radio bands (except 21.7 GHz) with the 0.1 – 0.3 and 0.3 – 1 GeV bands. At 10 – 100 GeV no correlation with any radio band was found for both types of blazars. Moreover, for FSRQs the correlation coefficient is more stable across the various energy bands in comparison with BL Lacs, for which Pearson’s r decreases faster for higher energy gamma-ray bands. If we examine correlation strength evolution across radio frequencies, BL Lacs showed a correlation of the same order at both 2.3 and 21.7 GHz with the flux in the 0.1 – 1 GeV range. FSRQs showed noticeably less correlation at 2.3 GHz, compared the correlation at 21.7 GHz, with the flux from the same gamma-ray range. Hence, we find that for BL Lac blazars, the correlation of the fluxes appears to be more sensitive to the considered gamma-ray energy band than to the frequency, while for FSRQ sources, the correlation changed both with the considered radio frequency and gamma-ray energy band.

3.2 Robustness test for the correlation

We used the permutation method described by Pavlidou et al. (2012) to test the significance of the computed correlation coefficients. It is intended to take account of common distance bias and Malmquist bias. Simulated samples contained only sources with known redshifts (because luminosities are used in this method) and thus the number of objects was reduced to 103 (48 BL Lacs and 55 FSRQs). We ran the permutation procedure 10^7 times. Thus, the probability to obtain Pearson’s r value more or equal to the real one from intrinsically uncorrelated measurements was calculated (hereinafter referred to as significance or *sig*). The results of the data randomization analysis are presented in Table 5, where we give the number of sources for each blazar subset (N), the value of the Pearson’s r , and the statistical significance of the apparent correlation (*sig*). Correlation coefficients are slightly different in some cases, from those given in Table 4, because only sources with known redshifts were involved in this robustness test.

We find that the highest significances occurs for higher correlation coefficients (e.g., $r=0.75$ with the chance probability

$sig=3.24 \times 10^{-7}$). The least significant cases are observed for the 10 – 100 GeV band for both types of blazar. Also there is a high probability for the correlation appearing by chance in the 1 – 3 and 3 – 10 GeV bands for FSRQs (up to 56 %). BL Lacs demonstrate only marginally significant correlation between the flux densities at 11.2 and 21.7 GHz and the photon flux at the 3 – 10 GeV band (2–6 % probability of achieving same or higher correlation from intrinsically uncorrelated data).

4 DISCUSSION AND CONCLUSIONS

We searched for a possible correlation between gamma-ray and radio emission in blazars. We used quasi-simultaneous multi-frequency *Fermi*-LAT and RATAN-600 observational data to test for the existence of the connection between fluxes in these bands. The correlation analysis was performed using the flux densities from five radio bands (2.3 – 21.7 GHz) for the first time. If the gamma-ray emission is produced by the SSC method, we would expect a tight correlation between gamma-ray and radio emission because the seed photons are produced by the same method. In previous work it is shown that SSC models are acceptable for most BL Lacs SEDs, while FSRQs usually require an external inverse Compton mechanism (e.g., Lindfors, Valtaoja & Türler 2005; Abdo et al. 2010a; Hovatta et al. 2014). Since SSC would imply the same origin for gamma-ray and radio emission, generally higher values of the correlation coefficient for BL Lacs were expected.

We found a positive apparent correlation between gamma-ray photon flux and radio flux density for sources from our sample, but with considerable scatter (Pearson’s r ranges from -0.03 to 0.74 for BL Lacs and from 0.03 to 0.57 for FSRQs). The BL Lacs show higher values of the correlation coefficient than FSRQs at all frequencies, except 21.7 GHz, and at all bands, except 10 – 100 GeV, when comparing different sub-samples of blazars. Also BL Lacs showed the correlation of the same order at both 2.3 and 21.7 GHz with the flux from the 0.1 – 1 GeV range, while FSRQs demonstrated noticeably less correlation at 2.3 GHz, compared with the correlation at 21.7 GHz, with the flux from the same gamma-ray range. At higher gamma-ray energies, the correlation weakens and even becomes negative for both BL Lacs and FSRQs, consistent with Ackermann et al. (2011). The strength of the correlation clearly depends on the gamma-ray energy band considered for both types of blazars; the correlation of the radio flux density at any frequency is stronger with the 0.1 – 1 GeV energy range. Thus, for BL Lac blazars, the correlation of the fluxes appeared to be more sensitive to the considered gamma-ray energy band, than to the frequency, while for FSRQ sources correlation seems to change both with the considered radio frequency and gamma-ray energy band.

We used data randomization tests to quantify the significance of the computed correlation coefficients. We find that the statistical significance of correlations we obtained between the flux densities at all frequencies and the photon flux at all gamma-ray bands below 3 GeV is high for BL Lacs (chance probability $\sim 10^{-3} - 10^{-7}$). The correlation coefficient is highly significant for 0.1 – 0.3 GeV and low and insignificant for the 10 – 100 GeV band for both types of blazars for all considered frequencies.

We used quasi-simultaneous data at radio frequencies; there was RATAN-600 data for the first year of operation of *Fermi*-LAT (within a few months). Simultaneity of the data used plays important role in analysis and as shown in previous works (e.g., Ackermann et al. 2011; León-Tavares et al. 2012) strength of the correlation depends on concurrency. Ackermann et al. (2011) re-

veal stronger correlation between gamma-ray and radio emission for concurrent data than for archival (comparing archival 8.4 GHz data and simultaneous 15 GHz measurements). León-Tavares et al. (2012) found higher statistical significance for the $L_\gamma - L_{radio}$ correlation in data obtained quasi-simultaneously (within months), than in simultaneous observations (within weeks) and in data averaged over a long-term period (27 months). Fuhrmann et al. (2014) analysed gamma-ray/radio light curves of 54 Fermi-bright blazars. They estimated 12 ± 8 d time lag at 3 mm wavelength. According to their study, the time delay systematically increases from the millimetre to the centimetre band. If the same beamed relativistic electrons first up-scatter the synchrotron photons to gamma-ray energies and then flare in the radio band, then a significant time delay between the radio and gamma-ray flares is expected. Also such time lags would occur, if a disturbance (a shock, propagating along the jet) appears from the radio core and first causes a flare in the (sub-)millimetre band and then produces a gamma-ray flare downstream in the jet. However, there is no commonly accepted physical model for the radio/gamma-ray emission regions: some studies suggest gamma-ray flare occurring downstream from the radio core, others, upstream from the core. Scenarios vary depending on the flare type (relatively strong or not), source type (BL Lacs and quasars) and radio band (mm, cm). The possible locations of the gamma-ray emission site are discussed in, for example, León-Tavares et al. (2011) and Fuhrmann et al. (2014) and references therein. Nonetheless, it is well known that there is a considerable delay between flares in radio and gamma-ray bands. That is why there are might be a larger chance of detecting a correlation in averaged radio and gamma-ray fluxes, than in simultaneous observational data.

Together with the previous results of the correlation between gamma-ray and radio band emission for AGNs (Ghirlanda et al. 2010; Kovalev et al. 2009; Ackermann et al. 2011), our results could be considered as suggesting the existence of a relationship between the emission from these bands, and as indication of the common origin (in terms of the assumed SSC radiation). Two possible radiation mechanisms, responsible for gamma-ray emission and SSC and external inverse Compton processes, probably always occur together, although in different proportions. Hence, it is difficult to provide sufficient reasons to conclude there is a direct and obvious link between gamma-ray and radio band emission in blazars.

ACKNOWLEDGEMENTS

The RATAN-600 observations were carried out with the financial support of the Ministry of Education and Science of the Russian Federation (state contract no.14.518.11.7054) and Russian Foundation for Basic Research (project no. 12-02-31649).

We thank the anonymous referee for useful comments and suggestions. The authors want to acknowledge S. Trushkin, V. Stolyarov and C. Riseley for the careful reading and help in preparing this manuscript. M. Mingaliev acknowledges support through the Russian Government Program of Competitive Growth of the Kazan Federal University.

We used on-line version of the Roma-BZCAT catalogue at the ASI Science Data Center (ASDC) website; therefore we are grateful to the ASDC staff.

This research made use of the NASA/IPAC Extragalactic Database (NED), which is operated by the Jet Propulsion Laboratory, California Institute of Technology, under contract with the National Aeronautics and Space Administration.

This research also has made use of the Vizier catalogue access tool, CDS, Strasbourg, France.

REFERENCES

- Abdo A. A., Ackermann M., Agudo I., Ajello M., Aller H. D., Aller M. F., Angelakis E., Arkharov A. A., 2010a, *ApJ*, 716, 30
 Abdo A. A. et al., 2010b, *ApJ*, 715, 429
 Abdo A. A. et al., 2010c, *ApJS*, 188, 405
 Ackermann M. et al., 2011, *ApJ*, 741, 30
 Blandford R. D., Levinson A., 1995, *ApJ*, 441, 79
 Bregman J. N., Glassgold A. E., Huggins P. J., Lebofsky M. J., Rieke G. H., Aller M. F., Aller H. D., Hodge P. E., 1981, *Nature*, 293, 714
 Fuhrmann L. et al., 2014, *MNRAS*, 441, 1899
 Ghirlanda G., Ghisellini G., Tavecchio F., Foschini L., 2010, *MNRAS*, 407, 791
 Hovatta T. et al., 2014, *MNRAS*, 439, 690
 Impey C. D., Neugebauer G., 1988, *AJ*, 95, 307
 Konigl A., 1981, *ApJ*, 243, 700
 Kovalev Y. Y. et al., 2009, *ApJ*, 696, L17
 León-Tavares J., Valtaoja E., Giommi P., Polenta G., Tornikoski M., Lähteenmäki A., Gasparrini D., Cutini S., 2012, *ApJ*, 754, 23
 León-Tavares J., Valtaoja E., Tornikoski M., Lähteenmäki A., Nieppola E., 2011, *A&A*, 532, A146
 Lindfors E. J., Valtaoja E., Türler M., 2005, *A&A*, 440, 845
 Marscher A. P., 1998, in *Astronomical Society of the Pacific Conference Series*, Vol. 144, IAU Colloq. 164: Radio Emission from Galactic and Extragalactic Compact Sources, Zensus J. A., Taylor G. B., Wrobel J. M., eds., p. 25
 Marscher A. P., Gear W. K., 1985, *ApJ*, 298, 114
 Massaro E., Giommi P., Leto C., Marchegiani P., Maselli A., Perri M., Piranomonte S., Scclavi S., 2009, *A&A*, 495, 691
 Mingaliev M. G., Sotnikova Y. V., Tornainen I., Tornikoski M., Udovitskiy R. Y., 2012, *A&A*, 544, 1
 Mingaliev M. G., Sotnikova Y. V., Udovitskiy R. Y., Mufakharov T. V., Nieppola E., Erkenov A. K., 2014, *A&A*, 572, A59
 Muecke A. et al., 1997, *A&A*, 320, 33
 Murphy T. et al., 2010, *MNRAS*, 402, 2403
 Nieppola E., Tornikoski M., Valtaoja E., León-Tavares J., Hovatta T., Lähteenmäki A., Tammi J., 2011, *A&A*, 535, A69
 Ott M., Witzel A., Quirrenbach A., Krichbaum T. P., Standke K. J., Schalinski C. J., Hummel C. A., 1994, *A&A*, 284, 331
 Padovani P., Ghisellini G., Fabian A. C., Celotti A., 1993, *MNRAS*, 260, L21
 Pavlidou V. et al., 2012, *ApJ*, 751, 149
 Richards J. L. et al., 2011, *ApJS*, 194, 29
 Rybicki G. B., Lightman A. P., 1979, *Radiative processes in astrophysics*
 Sambruna R. M., Maraschi L., Urry C. M., 1996, *ApJ*, 463, 444
 Sikora M., Begelman M. C., Rees M. J., 1994, *ApJ*, 421, 153
 Stecker F. W., Salamon M. H., Malkan M. A., 1993, *ApJ*, 410, L71
 Tabara H., Inoue M., 1980, *A&AS*, 39, 379
 Taylor G. B. et al., 2007, *ApJ*, 671, 1355
 Urry C. M., Mushotzky R. F., 1982, *ApJ*, 253, 38
 Urry C. M., Padovani P., 1995, *PASP*, 107, 803
 Verkhodanov O. V., 1997, *Astronomical Data Analysis Software and Systems VI*, A.S.P. Conference Series, 125, 46
 von Montigny C. et al., 1995, *ApJ*, 440, 525

6 *T. Mufakharov*

Wall J. V., Jenkins C. R., 2003, *Practical Statistics for Astronomers*, Ellis R., Huchra J., Kahn S., Rieke G., Stetson P. B., eds.

Table 2. List of objects

Name	Type	z	Name	Type	z
BZB J0022+0608	BL Lac	-	PKS 1118-05	FSRQ	1.297
BZB J0035+1515	BL Lac	1.28	FBQS J115019.2+241753	BL Lac	0.2
GC0039+23	FSRQ	1.426	4C 29.45	FSRQ	0.725
PKS 0047+023	BL Lac	1.44	EXO1218.8+3027	BL Lac	0.182
FBQS J0050-0929	BL Lac	0.103	ON 231	BL Lac	0.102
PKS 0106+01	FSRQ	2.099	PKS 1219+04	FSRQ	0.966
GC 0109+224	BL Lac	0.265	PKS 1222+21	FSRQ	0.435
BZQ J0136+4751	FSRQ	0.859	3C 273	FSRQ	0.158
PKS 0139-09	BL Lac	0.733	FBQS J123014.0+251807	BL Lac	0.135
2MASX J01593439+1047052	BL Lac cand	0.195	3C 279	FSRQ	0.53
4C +15.05	Blaz.uncer	0.833	1WGA J1310.4+3220	FSRQ	0.997
2MASS J02171711+0837038	BL Lac cand	1.4	GB6 J1327+2210	FSRQ	-
PKS 0215+015	FSRQ	1.715	PKS 1335-127	FSRQ	0.539
B2 0218+35	Blaz.uncer	0.944	FIRST J134105.1+395945	BL Lac	0.172
3C 66A	BL Lac	0.444	CGRaBS J1357+7643	FSRQ	1.585
BZQ J0237+2848	FSRQ	1.213	PKS 1406-076	FSRQ	1.494
PKS 0235+164	BL Lac	0.94	FBQS J142700.4+234800	BL Lac	0.16
2MASX J02503793+1712092	Blaz.uncer	1.1	2MASS J14424821+1200402	BL Lac	0.162
BZB J0303+4716	BL Lac	0.475	PKS 1502+106	FSRQ	1.839
BZB J0316+0904	BL Lac	-	PKS 1502+036	FSRQ	0.409
NGC 1275	Blaz.uncer	0.018	PKS 1510-08	FSRQ	0.36
BZB J0319+1845	BL Lac	0.19	PKS 1514+197	BL Lac	0.65
1H 0323+022	BL Lac	0.147	1RXS J152239.7-273025	BL Lac	1.294
PKS 0332-403	BL Lac cand	-	4C +05.64	FSRQ	1.422
NRAO 140	FSRQ	1.259	BZB J1555+1111	BL Lac	0.36
PKS 0336-017	FSRQ	0.85	SDSS J160706.23+155136.8	BL Lac	0.357
1H 0413+009	BL Lac	0.287	4C +10.45	FSRQ	1.226
PKS 0420+022	FSRQ	2.277	BZQ J1613+3412	FSRQ	1.399
PKS 0420-01	FSRQ	0.916	4C +38.41	FSRQ	1.813
PKS 0422+004	BL Lac	0.31	3C 345	FSRQ	0.593
PKS 0446+11	BL Lac	1.207	MRK 0501	BL Lac	0.033
PKS 0454-234	FSRQ	1.003	PKS 1717+177	BL Lac	0.137
4C-02.19	FSRQ	2.291	2MASS J17250434+1152155	BL Lac	0.018
BZQ J0505+0459	BL Lac cand	0.027	NRAO 530	FSRQ	0.902
2MASS J05075617+6737242	BL Lac	0.314	1ES 1741+196	BL Lac	0.083
BZB J0509+0541	BL Lac	0.304	OT 081	Blaz.uncer	0.322
PKS 0507+17	FSRQ	0.416	BZB J1756+5522	BL Lac	0.407
PKS 0539-057	FSRQ	0.839	BZB J1800+7828	BL Lac	0.68
OH-10	FSRQ	0.872	3C 380.0	Blaz.uncer	0.695
2MASS J06251826+4440014	BL Lac	-	BZQ J1852+4855	FSRQ	1.25
2MASX J07103005+5908202	BL Lac	0.125	PKS 1954-388	FSRQ	0.63
PKS 0723-008	Blaz.uncer	0.128	BZB J2005+7752	BL Lac	0.342
PKS 0735+17	BL Lac	0.424	PKS 2012-017	BL Lac	0.52
PKS 0736+01	FSRQ	0.189	BZQ J2035+1056	FSRQ	0.601
PKS 0748+126	FSRQ	0.889	PKS 2047+039	BL Lac cand	-
PKS 0754+100	BL Lac	0.266	PKS 2131-021	BL Lac	0.557
PKS 0805-07	FSRQ	1.837	BZQ J2143+1743	FSRQ	0.213
PKS 0808+019	BL Lac	0.93	4C 06.69	FSRQ	0.999
B3 0814+425	BL Lac	0.53	PKS 2149+173	BL Lac	0.871
PKS 0823+033	BL Lac	0.506	BL Lac	BL Lac	0.069
BZQ J0830+2410	FSRQ	0.941	PKS 2201+171	FSRQ	1.076
PKS 0829+046	BL Lac	0.18	PKS 2209+236	FSRQ	1.125
2EG J0852-1237	FSRQ	0.566	3C 446	FSRQ	1.404
PKS 0851+202	BL Lac	0.306	BZQ J2229-0832	FSRQ	1.56
BZQ J0920+4441	FSRQ	2.186	4C -11.69	FSRQ	1.037
2MASS J09303759+4950256	BL Lac	0.188	3C 454.3	FSRQ	0.859
OK 290	FSRQ	0.708	PKS 2254-204	BL Lac	-
2MASS J10121335+0630569	BL Lac	0.727	PKS2255-282	FSRQ	0.926
SDSS J101603.13+051302.3	FSRQ	1.713	BZB J2304+3705	BL Lac	-
FBQS J104309.0+240835	FSRQ	0.56	PKS 2320-035	FSRQ	1.393
4C01.28	Blaz.uncer	0.89	2MASS J23385638+2124410	BL Lac cand	0.291
2XMM J110427.3+381231	BL Lac	0.031			

Table 3: List of objects with their RATAN-600 flux density values (Jy) and spectral indices (α), measured between 2.3 and 7.7 GHz

Name	$\alpha_{2.3-7.7GHz}$	$F_{21.7GHz}$ (Jy)	$F_{11.2GHz}$ (Jy)	$F_{7.7GHz}$ (Jy)	$F_{4.8GHz}$ (Jy)	$F_{2.3GHz}$ (Jy)
BZB J0022+0608	-0.10	0.24 ± 0.009	0.38 ± 0.009	0.43 ± 0.011	0.48 ± 0.010	0.44 ± 0.021
BZB J0035+1515	-0.40	0.03 ± 0.007	0.02 ± 0.003	0.02 ± 0.003	0.02 ± 0.002	0.03 ± 0.005
GC0039+23	-0.29	0.36 ± 0.010	0.52 ± 0.021	0.60 ± 0.029	0.80 ± 0.028	0.95 ± 0.061
PKS 0047+023	-0.01	0.14 ± 0.020	0.19 ± 0.007	0.20 ± 0.007	0.23 ± 0.005	0.18 ± 0.009
FBQS J0050-0929	0.27	1.42 ± 0.022	1.32 ± 0.038	1.26 ± 0.027	1.06 ± 0.017	0.78 ± 0.029
PKS 0106+01	0.23	2.45 ± 0.187	2.43 ± 0.063	2.16 ± 0.074	1.83 ± 0.048	1.63 ± 0.088
GC 0109+224	0.24	0.45 ± 0.057	0.61 ± 0.022	0.61 ± 0.029	0.60 ± 0.022	0.43 ± 0.035
BZQ J0136+4751	0.43	4.22 ± 0.145	4.42 ± 0.166	4.63 ± 0.250	4.08 ± 0.178	2.45 ± 0.186
PKS 0139-09	-0.19	0.45 ± 0.016	0.55 ± 0.024	0.60 ± 0.013	0.74 ± 0.012	0.72 ± 0.031
2MASX J01593439+1047052	-1.15	–	0.02 ± 0.003	0.02 ± 0.003	0.04 ± 0.003	0.08 ± 0.010
4C +15.05	-0.61	0.74 ± 0.033	1.09 ± 0.042	1.36 ± 0.061	1.89 ± 0.058	2.85 ± 0.376
2MASS J02171711+0837038	-0.18	0.26 ± 0.011	0.44 ± 0.010	0.55 ± 0.015	0.61 ± 0.013	0.57 ± 0.023
PKS 0215+015	0.33	1.88 ± 0.025	1.90 ± 0.057	1.88 ± 0.057	1.65 ± 0.046	1.00 ± 0.075
B2 0218+35	-0.12	1.32 ± 0.018	1.50 ± 0.120	1.71 ± 0.070	1.59 ± 0.075	1.78 ± 0.103
3C 66A	-0.32	0.69 ± 0.064	0.96 ± 0.034	1.19 ± 0.050	1.27 ± 0.054	1.65 ± 0.133
BZQ J0237+2848	-0.10	1.89 ± 0.038	2.71 ± 0.089	2.86 ± 0.123	3.06 ± 0.108	3.16 ± 0.176
PKS 0235+164	0.32	4.44 ± 0.053	5.38 ± 0.133	5.54 ± 0.164	5.16 ± 0.127	2.90 ± 0.113
2MASX J02503793+1712092	-0.57	0.02 ± 0.008	0.03 ± 0.002	0.03 ± 0.002	0.04 ± 0.002	0.07 ± 0.016
BZB J0303+4716	0.31	0.99 ± 0.057	1.05 ± 0.039	1.17 ± 0.057	0.95 ± 0.059	0.71 ± 0.094
BZB J0316+0904	-0.08	0.07 ± 0.018	0.07 ± 0.005	0.07 ± 0.006	0.08 ± 0.003	0.08 ± 0.012
NGC 1275	0.83	15.63 ± 1.136	20.41 ± 0.732	19.00 ± 0.799	14.46 ± 0.778	17.00 ± 1.864
BZB J0319+1845	-0.83 ⁵	0.02 ± 0.010	0.03 ± 0.004	0.04 ± 0.005	0.04 ± 0.003	–
1H 0323+022	-0.72	0.02 ± 0.007	0.02 ± 0.003	0.03 ± 0.003	0.05 ± 0.002	0.08 ± 0.014
PKS 0332-403	0.72	2.12 ± 0.041	1.77 ± 0.108	1.46 ± 0.102	0.86 ± 0.059	0.45 ± 0.040
NRAO 140	-0.54	1.48 ± 0.129	1.16 ± 0.045	1.13 ± 0.054	1.54 ± 0.073	2.50 ± 0.195
PKS 0336-017	-0.03	1.86 ± 0.140	2.27 ± 0.108	2.47 ± 0.109	2.63 ± 0.135	2.47 ± 0.232
1H 0413+009	-0.70	0.03 ± 0.005	0.04 ± 0.003	0.05 ± 0.004	0.07 ± 0.002	0.11 ± 0.008
PKS 0420+022	-0.03	0.64 ± 0.044	0.97 ± 0.021	1.16 ± 0.028	1.23 ± 0.023	0.94 ± 0.029
PKS 0420-01	0.54	5.10 ± 0.477	4.75 ± 0.692	4.18 ± 0.607	3.22 ± 0.232	2.09 ± 0.212
PKS 0422+004	0.03	0.60 ± 0.015	0.68 ± 0.014	0.65 ± 0.016	0.66 ± 0.012	0.55 ± 0.024
PKS 0446+11	-0.11	0.72 ± 0.074	0.66 ± 0.053	0.67 ± 0.040	0.80 ± 0.044	0.88 ± 0.141
PKS 0454-234	0.06	2.08 ± 0.022	2.15 ± 0.072	2.23 ± 0.074	2.26 ± 0.087	2.13 ± 0.088
4C-02.19	0.07	1.03 ± 0.085	0.89 ± 0.062	0.90 ± 0.044	0.93 ± 0.025	0.85 ± 0.093
BZQ J0505+0459	-0.84	0.03 ± 0.005	0.06 ± 0.003	0.08 ± 0.005	0.12 ± 0.003	0.19 ± 0.014
2MASS J05075617+6737242	0.12 ⁵	0.05 ± 0.015	0.04 ± 0.008	0.04 ± 0.010	0.04 ± 0.006	–
BZB J0509+0541	-0.02	0.45 ± 0.020	0.67 ± 0.015	0.69 ± 0.018	0.70 ± 0.015	0.64 ± 0.022
PKS 0507+17	0.38	1.30 ± 0.019	1.17 ± 0.043	0.94 ± 0.045	0.71 ± 0.050	0.48 ± 0.064
PKS 0539-057	-0.02	1.08 ± 0.027	1.18 ± 0.107	1.30 ± 0.061	1.38 ± 0.035	1.22 ± 0.114
OH-10	-0.16	1.49 ± 0.146	–	0.98 ± 0.072	1.11 ± 0.028	1.33 ± 0.136
2MASS J06251826+4440014	-0.02	0.13 ± 0.014	0.21 ± 0.010	0.22 ± 0.013	0.20 ± 0.014	0.18 ± 0.030
2MASX J07103005+5908202	-0.88	0.12 ± 0.036	0.08 ± 0.011	0.07 ± 0.006	0.10 ± 0.009	0.19 ± 0.016
PKS 0723-008	0.25	2.26 ± 0.131	2.14 ± 0.062	2.18 ± 0.065	2.34 ± 0.052	1.52 ± 0.084
PKS 0735+17	-0.31	0.49 ± 0.011	0.75 ± 0.019	0.84 ± 0.026	0.96 ± 0.024	1.11 ± 0.045
PKS 0736+01	-0.08	1.32 ± 0.090	1.43 ± 0.045	1.48 ± 0.062	1.59 ± 0.062	1.58 ± 0.260
PKS 0748+126	0.36	3.65 ± 0.112	4.18 ± 0.112	4.13 ± 0.164	3.68 ± 0.206	2.49 ± 0.282
PKS 0754+100	0.02	0.93 ± 0.015	1.02 ± 0.023	1.03 ± 0.027	0.98 ± 0.021	0.92 ± 0.034
PKS 0805-07	0.86	1.54 ± 0.119	0.97 ± 0.143	0.85 ± 0.039	0.39 ± 0.028	0.59 ± 0.076
PKS 0808+019	0.77	1.15 ± 0.018	1.04 ± 0.021	0.83 ± 0.020	0.49 ± 0.009	0.31 ± 0.014
B3 0814+425	0.25	1.32 ± 0.184	1.70 ± 0.049	1.81 ± 0.087	1.52 ± 0.080	1.20 ± 0.135
PKS 0823+033	0.38	1.87 ± 0.028	1.95 ± 0.041	1.74 ± 0.042	1.38 ± 0.026	1.07 ± 0.049
BZQ J0830+2410	0.37	1.09 ± 0.173	1.48 ± 0.062	1.46 ± 0.059	1.29 ± 0.121	0.85 ± 0.163
PKS 0829+046	-0.08	0.55 ± 0.038	0.59 ± 0.021	0.59 ± 0.018	0.59 ± 0.030	0.68 ± 0.199
2EG J0852-1237	0.41	0.83 ± 0.048	0.73 ± 0.034	0.64 ± 0.022	0.45 ± 0.046	0.38 ± 0.074
PKS 0851+202	0.63	3.81 ± 0.165	3.44 ± 0.111	2.65 ± 0.114	1.95 ± 0.073	1.24 ± 0.090

⁵ measured between 4.8 and 7.7 GHz

Table 3: continue

Name	$\alpha_{2.3-7.7GHz}$	$F_{21.7GHz}$ (Jy)	$F_{11.2GHz}$ (Jy)	$F_{7.7GHz}$ (Jy)	$F_{4.8GHz}$ (Jy)	$F_{2.3GHz}$ (Jy)
BZQ J0920+4441	0.39	2.20 ± 0.146	1.81 ± 0.058	1.50 ± 0.053	1.08 ± 0.045	0.99 ± 0.052
2MASS J09303759+4950256	-0.71	–	0.06 ± 0.014	0.06 ± 0.009	0.07 ± 0.013	0.16 ± 0.019
OK 290	-0.20	0.62 ± 0.041	0.70 ± 0.027	0.71 ± 0.035	0.83 ± 0.039	0.97 ± 0.133
2MASS J10121335+0630569	-0.49	0.13 ± 0.012	0.20 ± 0.006	0.23 ± 0.008	0.32 ± 0.011	0.44 ± 0.021
SDSS J101603.13+051302.3	0.11	0.68 ± 0.012	0.71 ± 0.020	0.68 ± 0.029	0.69 ± 0.028	0.62 ± 0.068
FBQS J104309.0+240835	0.08	0.41 ± 0.009	0.60 ± 0.017	0.67 ± 0.023	0.74 ± 0.021	0.57 ± 0.025
4C01.28	0.20	4.52 ± 0.147	4.09 ± 0.102	3.57 ± 0.104	3.20 ± 0.084	2.98 ± 0.322
2XMM J110427.3+381231	-0.36	0.29 ± 0.010	0.41 ± 0.013	0.48 ± 0.019	0.53 ± 0.019	0.68 ± 0.034
PKS 1118-05	-0.31	0.33 ± 0.016	0.45 ± 0.022	0.55 ± 0.012	0.75 ± 0.014	0.87 ± 0.033
FBQS J115019.2+241753	0.04	0.56 ± 0.015	0.73 ± 0.020	0.78 ± 0.027	0.82 ± 0.024	0.71 ± 0.031
4C 29.45	0.17	1.92 ± 0.110	2.65 ± 0.084	2.68 ± 0.115	2.71 ± 0.092	2.07 ± 0.178
EXO1218.8+3027	-0.57	0.02 ± 0.005	0.03 ± 0.003	0.04 ± 0.004	0.05 ± 0.002	0.08 ± 0.013
ON 231	0.09	0.33 ± 0.078	0.43 ± 0.025	0.44 ± 0.025	0.49 ± 0.017	0.38 ± 0.067
PKS 1219+04	0.36	1.04 ± 0.105	1.06 ± 0.058	0.82 ± 0.044	0.64 ± 0.013	0.56 ± 0.076
PKS 1222+21	-0.33	0.76 ± 0.120	1.13 ± 0.041	1.18 ± 0.056	1.31 ± 0.067	1.80 ± 0.182
3C 273	-0.27	21.63 ± 1.771	28.48 ± 0.660	32.85 ± 1.606	39.02 ± 1.006	44.79 ± 3.988
FBQS J123014.0+251807	-0.24	0.11 ± 0.008	0.16 ± 0.005	0.18 ± 0.007	0.23 ± 0.007	0.24 ± 0.015
3C 279	0.26	13.66 ± 0.615	12.67 ± 0.447	11.85 ± 0.305	10.84 ± 0.240	8.51 ± 0.341
1WGA J1310.4+3220	0.32	1.79 ± 0.063	1.60 ± 0.054	1.34 ± 0.059	1.11 ± 0.041	0.93 ± 0.173
GB6 J1327+2210	-0.32	0.52 ± 0.070	0.77 ± 0.035	0.91 ± 0.043	1.16 ± 0.041	1.31 ± 0.162
PKS 1335-127	0.50	5.77 ± 0.057	4.97 ± 0.143	4.83 ± 0.280	3.91 ± 0.163	2.12 ± 0.104
FIRST J134105.1+395945	-0.98	–	0.02 ± 0.004	0.02 ± 0.004	0.04 ± 0.004	0.09 ± 0.021
CGRaBS J1357+7643	-0.05	0.55 ± 0.016	0.76 ± 0.031	0.82 ± 0.032	0.87 ± 0.042	0.78 ± 0.061
PKS 1406-076	0.15	0.77 ± 0.074	0.75 ± 0.071	0.78 ± 0.028	0.71 ± 0.018	0.61 ± 0.082
FBQS J142700.4+234800	-0.23	0.18 ± 0.011	0.28 ± 0.008	0.31 ± 0.011	0.37 ± 0.011	0.38 ± 0.021
2MASS J14424821+1200402	-0.49	0.02 ± 0.006	0.03 ± 0.002	0.03 ± 0.002	0.04 ± 0.002	0.06 ± 0.010
PKS 1502+106	0.48	3.32 ± 0.103	2.79 ± 0.081	2.29 ± 0.079	1.65 ± 0.046	1.29 ± 0.092
PKS 1502+036	-0.01	0.53 ± 0.018	0.60 ± 0.032	0.62 ± 0.028	0.63 ± 0.031	0.57 ± 0.023
PKS 1510-08	0.14	2.48 ± 0.204	2.16 ± 0.244	1.80 ± 0.069	1.83 ± 0.047	1.84 ± 0.284
PKS 1514+197	0.75	1.22 ± 0.017	1.18 ± 0.031	0.99 ± 0.031	0.74 ± 0.019	0.37 ± 0.018
1RXS J152239.7-273025	0.10	0.65 ± 0.022	0.85 ± 0.030	0.99 ± 0.062	1.12 ± 0.066	0.94 ± 0.133
4C +05.64	-0.06	2.59 ± 0.094	3.00 ± 0.072	3.20 ± 0.100	3.54 ± 0.096	3.34 ± 0.186
BZB J1555+1111	-0.34	0.12 ± 0.010	0.16 ± 0.005	0.18 ± 0.007	0.19 ± 0.005	0.26 ± 0.016
SDSS J160706.23+155136.8	-0.27	0.29 ± 0.012	0.38 ± 0.010	0.39 ± 0.012	0.44 ± 0.011	0.52 ± 0.022
4C +10.45	-0.25	0.98 ± 0.037	1.25 ± 0.043	1.32 ± 0.052	1.45 ± 0.042	1.81 ± 0.154
BZQ J1613+3412	-0.25	1.90 ± 0.095	3.12 ± 0.112	3.45 ± 0.154	3.84 ± 0.146	4.58 ± 0.685
4C +38.41	0.12	2.29 ± 0.117	2.90 ± 0.091	2.95 ± 0.124	2.94 ± 0.115	2.47 ± 0.144
3C 345	0.38	6.71 ± 0.245	7.25 ± 0.234	6.54 ± 0.273	5.90 ± 0.241	6.99 ± 0.652
MRK 0501	0.07	0.94 ± 0.042	1.31 ± 0.040	1.43 ± 0.059	1.46 ± 0.057	1.49 ± 0.102
PKS 1717+177	0.00	0.43 ± 0.015	0.58 ± 0.015	0.62 ± 0.020	0.60 ± 0.016	0.55 ± 0.025
2MASS J17250434+1152155	-0.55	0.04 ± 0.008	0.05 ± 0.004	0.05 ± 0.005	0.06 ± 0.003	0.10 ± 0.012
NRAO 530	0.12	4.57 ± 0.165	4.76 ± 0.104	4.45 ± 0.125	4.03 ± 0.078	3.85 ± 0.179
1ES 1741+196	-0.64	0.10 ± 0.005	0.14 ± 0.005	0.17 ± 0.007	0.21 ± 0.006	0.38 ± 0.019
OT 081	0.59	5.58 ± 0.065	5.35 ± 0.120	4.42 ± 0.116	3.16 ± 0.068	1.60 ± 0.063
BZB J1756+5522	-0.95	–	0.06 ± 0.009	0.05 ± 0.008	0.06 ± 0.008	0.22 ± 0.040
BZB J1800+7828	0.18	3.32 ± 0.038	2.85 ± 0.102	2.79 ± 0.090	2.71 ± 0.112	1.97 ± 0.107
3C 380.0	-0.63	2.97 ± 0.115	3.44 ± 0.094	4.04 ± 0.130	5.32 ± 0.210	9.03 ± 0.643
BZQ J1852+4855	-0.15	0.25 ± 0.107	0.22 ± 0.033	0.21 ± 0.031	0.23 ± 0.014	0.27 ± 0.022
PKS 1954-388	-0.10	1.20 ± 0.025	1.92 ± 0.089	2.19 ± 0.085	2.37 ± 0.103	2.14 ± 0.115
BZB J2005+7752	0.11	0.88 ± 0.018	0.89 ± 0.043	0.89 ± 0.030	0.86 ± 0.037	0.78 ± 0.046
PKS 2012-017	-0.32	0.30 ± 0.012	0.44 ± 0.010	0.48 ± 0.012	0.58 ± 0.011	0.68 ± 0.022
BZQ J2035+1056	-0.34	0.32 ± 0.016	0.38 ± 0.010	0.42 ± 0.013	0.57 ± 0.013	0.69 ± 0.026
PKS 2047+039	-0.17	0.42 ± 0.008	0.64 ± 0.014	0.69 ± 0.017	0.73 ± 0.015	0.77 ± 0.026
PKS 2131-021	-0.08	1.91 ± 0.021	2.22 ± 0.043	2.29 ± 0.051	2.51 ± 0.043	2.39 ± 0.070
BZQ J2143+1743	0.29	0.74 ± 0.080	1.02 ± 0.035	1.04 ± 0.052	0.96 ± 0.030	0.67 ± 0.093
4C 06.69	0.30	4.52 ± 0.567	5.52 ± 0.178	5.72 ± 0.169	5.59 ± 0.154	3.65 ± 0.181
PKS 2149+173	-0.28	0.35 ± 0.016	0.54 ± 0.015	0.60 ± 0.019	0.68 ± 0.018	0.77 ± 0.036
BL Lac	0.28	2.88 ± 0.330	3.72 ± 0.314	3.85 ± 0.242	3.06 ± 0.140	2.46 ± 0.149

Table 3: continue

Name	$\alpha_{2.3-7.7GHz}$	$F_{21.7GHz}$ (Jy)	$F_{11.2GHz}$ (Jy)	$F_{7.7GHz}$ (Jy)	$F_{4.8GHz}$ (Jy)	$F_{2.3GHz}$ (Jy)
PKS 2201+171	0.44	0.62 ± 0.031	0.80 ± 0.026	0.73 ± 0.042	0.68 ± 0.041	0.87 ± 0.067
PKS 2209+236	0.03	0.68 ± 0.016	0.91 ± 0.034	0.98 ± 0.042	1.07 ± 0.053	0.79 ± 0.095
3C 446	0.18	6.59 ± 0.351	7.87 ± 0.395	7.53 ± 0.228	6.85 ± 0.159	5.89 ± 0.196
BZQ J2229-0832	0.35	2.31 ± 0.168	2.41 ± 0.175	2.42 ± 0.085	2.40 ± 0.059	1.48 ± 0.135
4C -11.69	-0.12	4.10 ± 0.402	4.25 ± 0.275	4.27 ± 0.152	4.58 ± 0.156	5.32 ± 0.296
3C 454.3	-0.03	14.11 ± 0.159	11.79 ± 0.893	10.79 ± 0.350	10.18 ± 0.476	12.44 ± 0.546
PKS 2254-204	0.19	1.08 ± 0.030	1.00 ± 0.025	1.06 ± 0.042	1.04 ± 0.091	0.75 ± 0.090
PKS 2255-282	0.67	3.58 ± 0.037	2.80 ± 0.096	2.75 ± 0.108	2.21 ± 0.143	1.09 ± 0.052
BZB J2304+3705	-0.71	0.02 ± 0.003	0.02 ± 0.002	0.01 ± 0.002	0.02 ± 0.001	0.04 ± 0.005
PKS 2320-035	0.07	0.92 ± 0.051	1.01 ± 0.057	1.04 ± 0.038	1.05 ± 0.032	0.93 ± 0.061
2MASS J23385638+2124410	-0.73	0.02 ± 0.004	0.02 ± 0.002	0.02 ± 0.002	0.04 ± 0.002	0.06 ± 0.012

Table 4. Pearson’s r for broadband gamma-ray emission (photon fluxes at five bands 0.1 – 100 GeV) and radio emission (flux densities at five frequencies 2.3 – 21.7 GHz). For each frequency the number of sources (N) and typical confidence level values for correlation in this bands (CL) are presented. In Figure 3 we show the correlation coefficient distribution across the five energy bands and five frequencies, reported in this table.

Source class	N	0.1–0.3 GeV	0.3–1 GeV	1–3 GeV	3–10 GeV	10–100 GeV
21.7 GHz						
BL Lac	50	+0.61	+0.53	+0.43	+0.25	−0.03
FSRQ	56	+0.57	+0.46	+0.39	+0.26	+0.23
11.2 GHz						
BL Lac	53	+0.69	+0.62	+0.51	+0.32	+0.01
FSRQ	55	+0.47	+0.36	+0.28	+0.16	+0.16
7.7 GHz						
BL Lac	53	+0.73	+0.67	+0.56	+0.36	+0.04
FSRQ	56	+0.42	+0.31	+0.23	+0.11	+0.11
4.8 GHz						
BL Lac	53	+0.74	+0.69	+0.59	+0.39	+0.06
FSRQ	56	+0.39	+0.26	+0.18	+0.07	+0.07
2.3 GHz						
BL Lac	51	+0.64	+0.64	+0.55	+0.39	+0.14
FSRQ	56	+0.39	+0.26	+0.18	+0.05	+0.03
CL						
BL Lac		99%	99%	99%	99%	<90%
FSRQ		99%	95%	90%	<90%	<90%

Table 5. Pearson’s r for the radio flux density and gamma-ray photon fluxes with their significances (sig), calculated from data randomization analysis, for sources with known redshift (their number marked with N).

E (GeV)		0.1–0.3		0.3–1		1–3		3–10		10–100	
Source class	N	r	sig	r	sig	r	sig	r	sig	r	sig
21.7 GHz											
BL Lac	45	+0.61	5.29×10^{-7}	+0.53	3.76×10^{-5}	+0.42	1.13×10^{-3}	+0.24	0.055	−0.05	0.629
FSRQ	55	+0.56	6.26×10^{-7}	+0.46	9.79×10^{-5}	+0.39	1.13×10^{-3}	+0.26	0.023	+0.23	0.043
11.2 GHz											
BL Lac	48	+0.70	4.14×10^{-7}	+0.62	1.32×10^{-6}	+0.51	8.21×10^{-5}	+0.31	0.016	−0.003	0.934
FSRQ	54	+0.47	7.74×10^{-5}	+0.36	2.47×10^{-3}	+0.28	0.016	+0.16	0.134	+0.15	0.15
7.7 GHz											
BL Lac	48	+0.74	3.36×10^{-7}	+0.67	4.28×10^{-7}	+0.56	1.38×10^{-5}	+0.35	6.54×10^{-3}	+0.03	0.796
FSRQ	55	+0.42	4.21×10^{-4}	+0.30	9.68×10^{-3}	+0.23	0.048	+0.11	0.278	+0.11	0.288
4.8 GHz											
BL Lac	48	+0.75	3.24×10^{-7}	+0.69	4.06×10^{-7}	+0.58	5.44×10^{-6}	+0.38	3.14×10^{-3}	+0.05	0.632
FSRQ	55	+0.39	1.28×10^{-3}	+0.26	0.025	+0.18	0.104	+0.07	0.478	+0.07	0.480
2.3 GHz											
BL Lac	46	+0.63	4.87×10^{-7}	+0.63	4.94×10^{-7}	+0.54	2.35×10^{-5}	+0.38	2.87×10^{-3}	+0.13	0.28
FSRQ	55	+0.39	1.08×10^{-3}	+0.26	0.025	+0.18	0.110	+0.05	0.562	+0.04	0.695

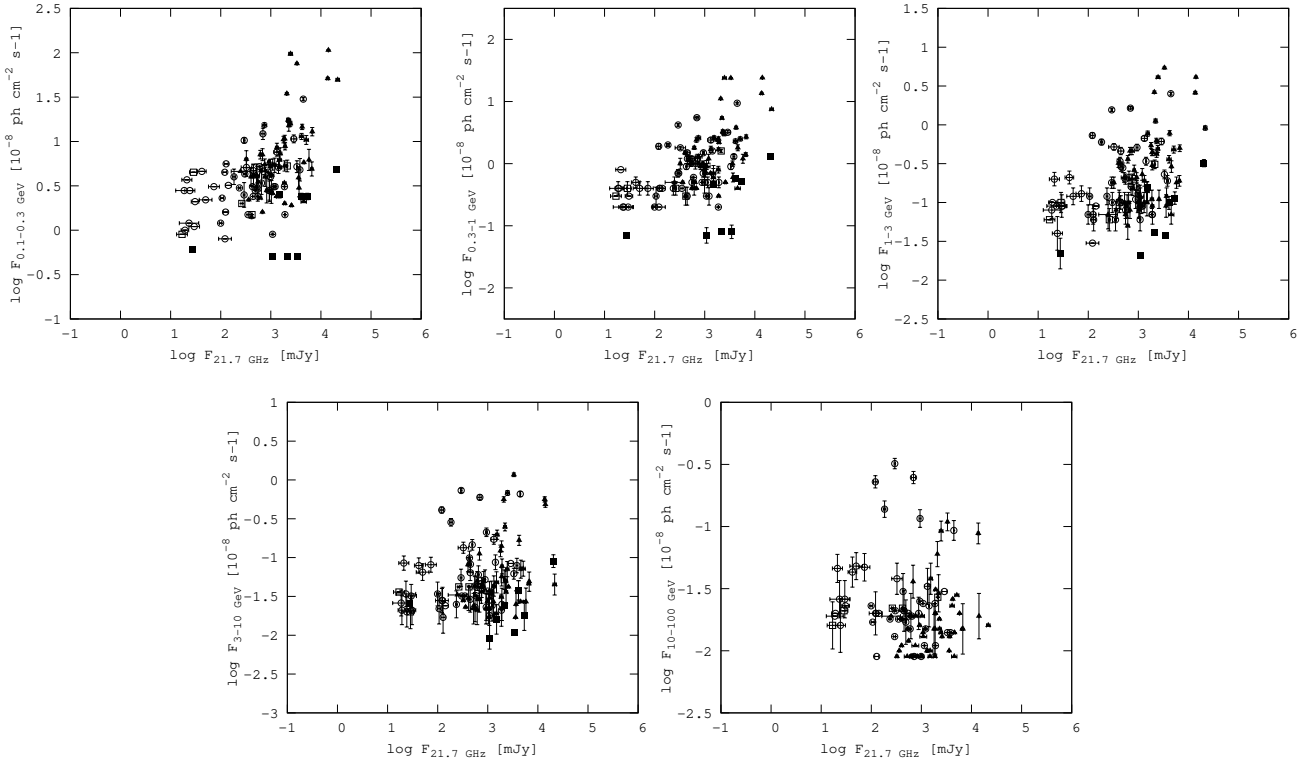


Figure 4. Broadband gamma-ray photon flux versus 21.7 GHz flux density. BL Lacs shown with empty circles, FSRQ - filled triangles, BL Lac candidates - empty squares, Blazars of uncertain type - filled squares.

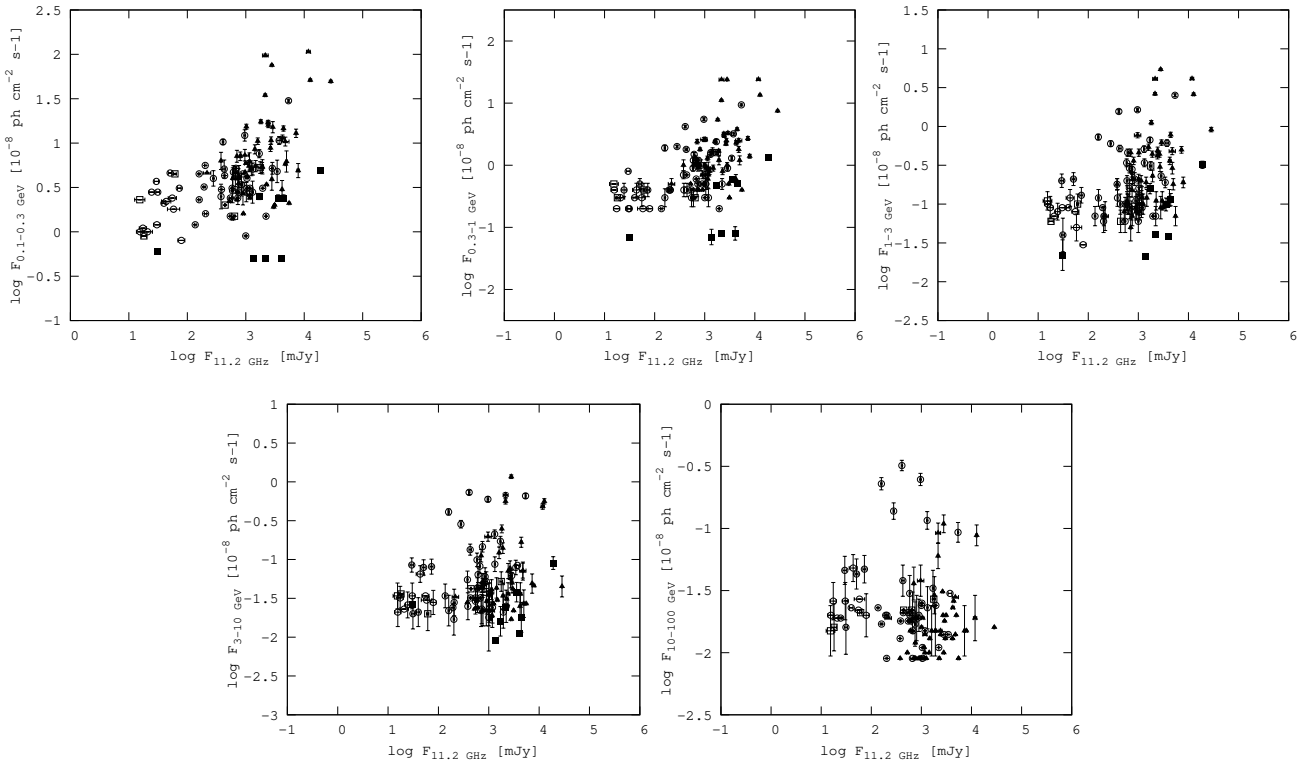


Figure 5. Broadband gamma-ray photon flux versus 11.2 GHz flux density. Designations are the same as in Fig 4

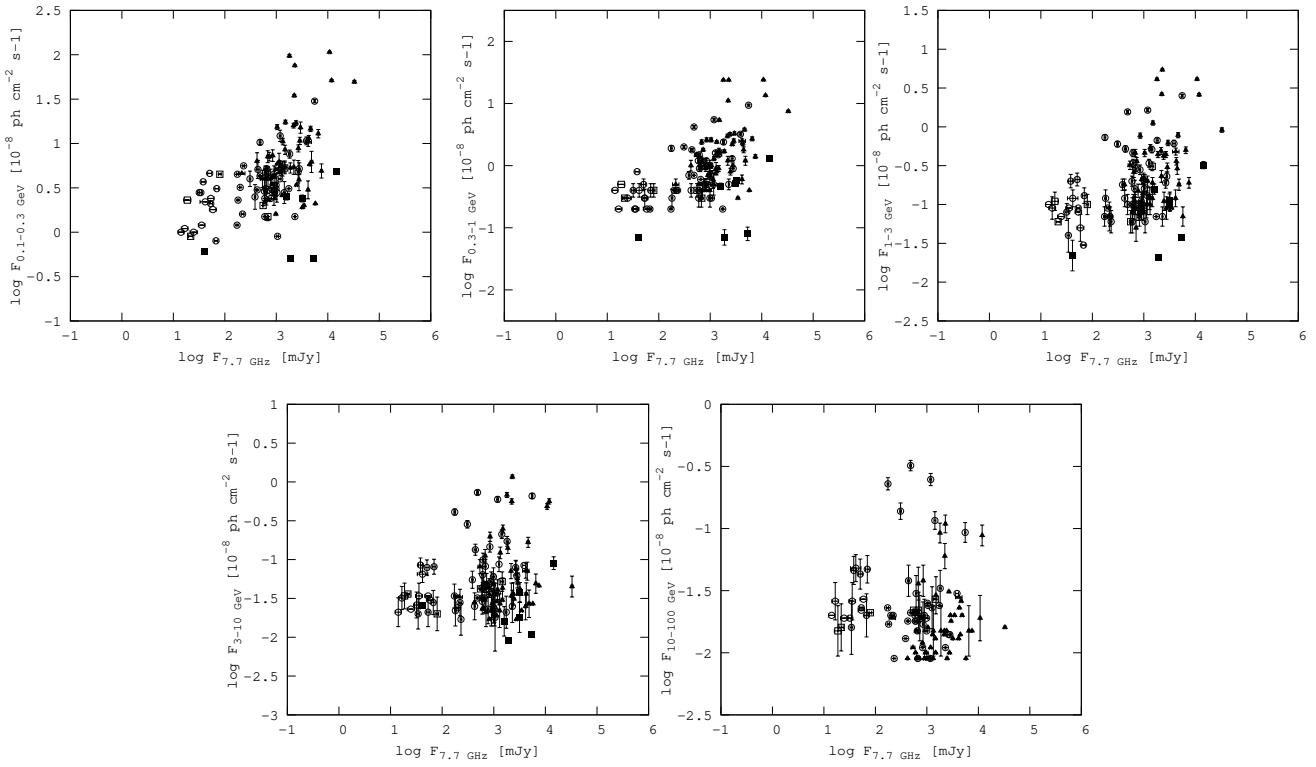


Figure 6. Broadband gamma-ray photon flux versus 7.7 GHz flux density. Designations are the same as in Fig 4

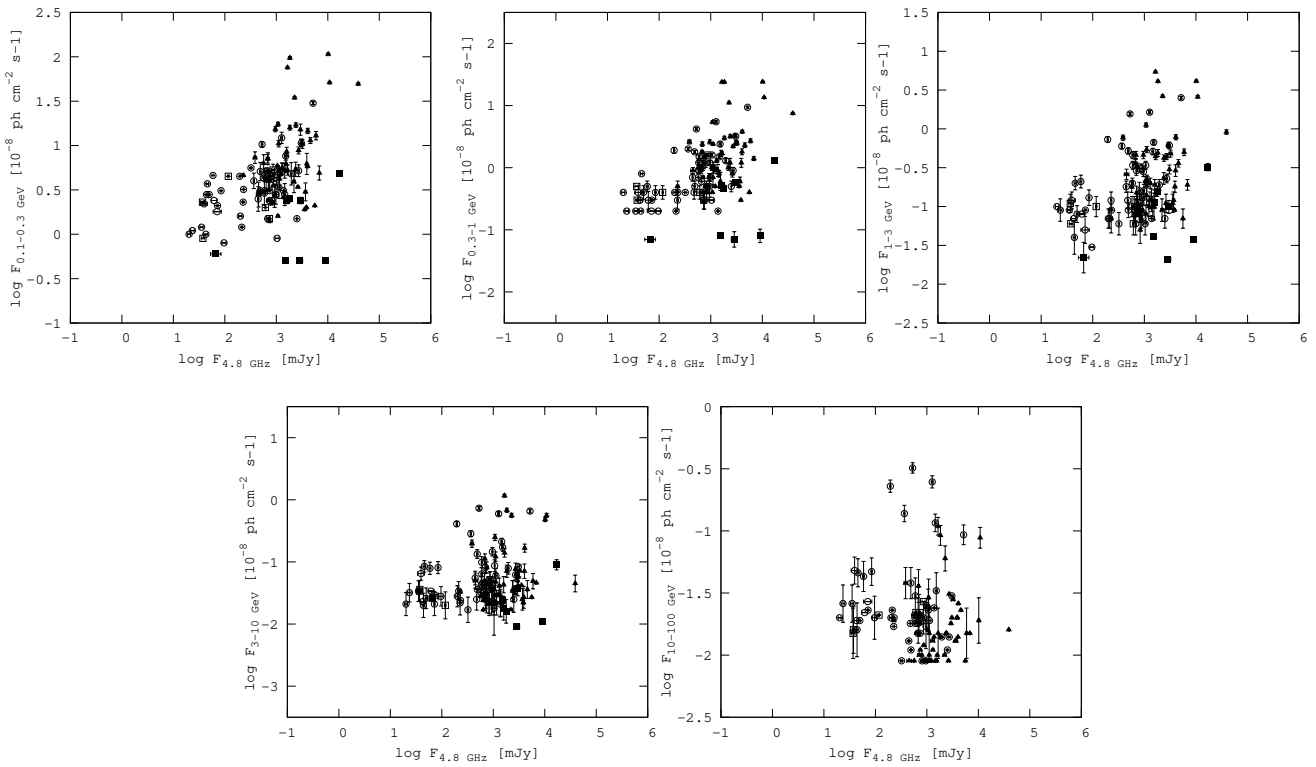


Figure 7. Broadband gamma-ray photon flux versus 4.8 GHz flux density. Designations are the same as in Fig 4

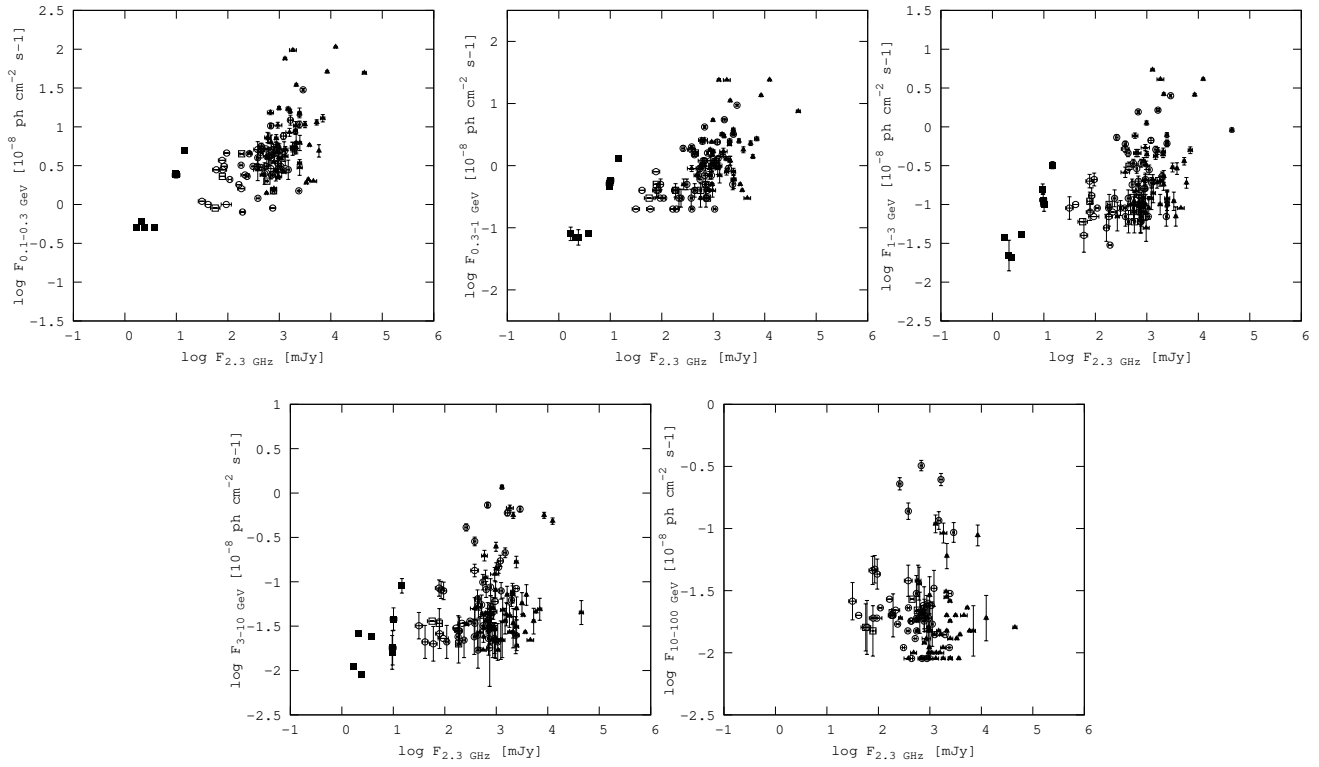


Figure 8. Broadband gamma-ray photon flux versus 2.3 GHz flux density. Designations are the same as in Fig 4